Spin depolarization for excitons in quantum wires

D. Larousserie and R. Ferreira
Laboratoire de Physique de la Matière Condensée, Ecole Normale Supérieure, 24 Rue Lhomond, F-75005 Paris, France
(Received 14 September 1998; revised manuscript received 16 February 1999)

We consider theoretically the exchange coupling for independent excitons in quantum wires. The one-dimensional dispersions are complicated because the confinement energy due to the wire and the kinetic energy along the wire axis are comparable in such structures. For weakly confining structures, we discuss different contributions for the spin depolarization in the presence of spin-conserving scatterings, which depend on the exchange couplings between the various confined center-of-mass exciton motions. We also find that the spin coupling for free excitons increases with decreasing wire cross sections in the strong confinement regime. Finally, we show for a gas of independent excitons that the localization effects increase the spin-depolarization time and alters its temperature dependence. [S0163-1829(99)08227-2]

I. INTRODUCTION

The fine structure of the exciton levels in bulk semiconductors is governed by the spin-dependent exchange interaction, which has two distinct parts: the analytical and the nonanalytical contributions. For a review of the main spin-dependent features related to the exchange coupling in bulk semiconductors, see for instance, Ref. 1. Various recent experimental and theoretical works are devoted to the study of the role played by the confinement on the spin relaxation of excitons in semiconductor quantum wells.[2,3] Maialle *et al.* have deduced the effective exchange Hamiltonian acting on the ground-heavy excitons of a quantum well.[2] For these structures, one diagonalizes the bulk exchange coupling on the basis of the pure-spin exciton levels with the same in-plane center-of-mass wave vector $\mathbf{K}_\perp=(K_X,K_Y)$. In fact, the translation invariance implies that only states with the same in-plane free motion are coupled by the exchange interaction. Also, for thin wells one can neglect the analytical term which introduces only weak nonresonant couplings between the low-lying heavy states with excited light excitons. In addition, the resonant nonanalytical interaction between the heavy excitons does not couple the optically ''active'' [$\sigma=\pm1$ (Ref. 4)] and the inactive ($\sigma=\pm2$) states. Under these approximations one obtains the effective exchange Hamiltonian acting on the only active ground-heavy excitons of a thin quantum well by averaging the nonanalytical bulk exchange perturbation over the independent electron and hole confined motions in the well and over the $1S$-like relative motion for the electron/hole pair. Maialle *et al.*[2] obtained a spin-diagonal term proportional to $K_\perp$ and a spin-mixing term proportional to $(K_X\pm iK_Y)^2/K_\perp$, besides a $K_\perp$-dependent form factor $\mathsf{F}(K_\perp)$ reflecting the electron and hole independent confinements by the quantum well potentials (with $\mathsf{F}[0]\approx1$). Thus, for thin wells, the diagonal and spin-mixing exchange couplings between the optically active ±1 ground-heavy exciton states are equal in magnitude and roughly proportional to the in-plane exciton wave vector $K_\perp$.[5] Various experimental works were reported concerning the spin depolarization of photocreated excitons in intrinsic wells [see for instance Ref. 3 and references therein]. One generally assumes that the exchange-related spin coupling is weak enough, as compared to the scattering broadening, implying a motional narrowing-like regime for the spin depolarization. In this regime, for a nondegenerate gas of independent excitons, the linear-in-$K_\perp$ (Ref. 5) coupling leads to a linear-in-T dependence for the spin-depolarization rate with temperature.

We consider theoretically in this work the exchange coupling for excitons in two different quantum wire structures: (i) in weakly confining wires (such as the ones built out of a thin quantum well by, say, a lithographic technique[6]) and (ii) in strongly confining wires (such as the ones obtained by direct growth on a substrate, as in V-groove structures[7]). By weak or strong confinement we mean that the energy shift of the low-lying exciton levels due to the wire perturbation is small or large as compared to the binding energy of the ground exciton of the underlying quantum well exciton. In the first case, one assumes that only the center-of-mass motion is affected by the wire potentials: this is the confined center-of-mass (CCM) regime. In the second case, the electron and hole confinements are independent: confined electron and hole (CEH) regime. The motion is free along the wire axis and, in the absence of spin-dependent couplings, a one-dimensional parabolic dispersion is associated to each CCM or CEH level. The wire states then form a series of one-dimensional subbands.

Let us take the free wire axis along the Y direction. The CCM levels can be thought of as formed by combining, say, the $+K_X$ and $-K_X$ quantum well plane waves. At $K_Y=0$, the single well exchange coupling is the same for the $\pm K_X$ propagative states. Consequently, as we show below, the edge states of the wire subbands are spin lifted. This is in striking contrast to the quantum well case where the spin splitting vanishes at the two-dimensional subband edge. With respect to the spin depolarization at low temperatures (low enough compared to the wire confinement energy and such that, say, only the ground wire subband is populated), this important result has two main consequences: (i) the calculated exciton spin-depolarization time does not diverge, as in the quantum well case, but is governed by the exchange coupling of the ground subband edge; (ii) increasing the wire confinement leads to a larger spin splitting of the wire edge states and thus to a larger spin-depolarization rate. The exci-

ton levels and spin depolarization in the weak confinement regime are discussed in Sec. II and Sec. III. We show in Sec. IV that similar results are obtained in the strong confinement regime. Finally, the effect of localization on the spin-depolarization rate is discussed in Sec. IV within a simple model.

II. WEAKLY CONFINING WIRES: ENERGY DISPERSIONS

For weakly confining quantum wires we assume that the relative motion of the electron-hole pair is ''frozen'' in the $1S$ quantum well state and only the center-of-mass motion is affected by the wire perturbations for the electron and hole. The exact form of the confining wire potentials depends on the growth parameters.[6,7] In order to evaluate the role of the weak one-dimensional confinement on the spin properties, we consider here two particular profiles for the center-of-mass confinement along, say, the x direction: a parabolic wire and a hard square well wire. Within the effective mass approximation, in the absence of exchange interaction, the low-lying heavy exciton (pure spin) levels of the wire read[8]

$$\Psi = \phi(z_e)\chi(z_h)\psi_{1S}(\rho)F_n(X)\exp(iK_Y Y)/\sqrt{L_Y}, \quad (1a)$$

$$\varepsilon_n(K_Y) = E_e + E_h - E_{1S} + E_n + \hbar^2 K_Y^2/2M, \quad (1b)$$

where the first two terms account for the ground confined electron and heavy hole levels of the well (confinement energies E_e and E_h, respectively), the third one for the relative motion (binding energy E_{1S}),[9] the fourth one for the confined center-of-mass (CCM) states and, finally, the last one for the free center-of-mass motion along the wire axis. The CCM energies are, to a good approximation, $E_n = \eta_n \hbar^2/(2ML_X^2)$ with $\eta_n = (2n-1)\sqrt{(M/\mu)}$ ($\eta_n = n^2\pi^2$) for the parabolic (vertical) wire;[8] $n \geqslant 1$; M and μ are the total and reduced in-plane exciton masses; L_X is the effective wire width. We assume for the relative motion a variational wave function: $\psi_\lambda(\rho) = N_\lambda \exp(-\rho/\lambda)$ where λ is the variational parameter and N_λ the normalization constant.[9] In the weak confinement or center-of-mass confinement regime there is $L_X \gg \lambda$ ($\approx$100 Å for GaAs based structures). The heavy states in Eq. (1) are fourfold degenerate when we consider the electron and hole spins ($\sigma = \pm 1, \pm 2$ for the z component of the exciton spin). For a given underlying quantum well (fixed z_e, z_h and relative electron-hole motions) the quantum wire states are specified by three quantum numbers, $|n;\sigma;K_Y\rangle$, and are organized in a (dense) series of parabolic dispersions as function of K_Y. In the calculations below we use the following parameters (which correspond to those of the GaAs). Position independent masses: $m_{E(X,Y,Z)} = 0.067 m_0$; $m_{H(X,Y)} \approx 0.11 m_0$ and $m_{H(Z)} \approx 0.38 m_0$. The position independent relative dielectric constant is equal to 12.5 in the calculation of the ground exciton level. Offset discontinuities: $V_E \approx 277$ meV and $V_H \approx 142$ meV (except in the last section, where these discontinuities are assumed infinite). The subscript ''E'' holds for electrons and ''H'' for heavy holes.

In the following we diagonalize the exchange coupling[10] on the basis of the pure spin exciton levels with fixed K_Y [Eq. (1a)]. In fact, only states with the same free motion along the wire axis are coupled by the exchange interaction. In addition, we neglect the analytical term, which introduces weak nonresonant couplings between the low-lying heavy states we are interested in here with excited light exciton states. We neglect also the inactive heavy states ($\sigma = \pm 2$ dispersions), which are not coupled to the optically ''active'' [$\sigma = \pm 1$ (Ref. 4)] ones by the resonant nonanalytical interaction. Finally, for each K_Y value, the numerical basis for the calculations is spanned by the $2N$ states $|n = 1,...,N;\ \sigma = \pm 1;\ K_Y\rangle$ with N large enough to ensure a convergence for the first few mixed states. In this basis, the nonanalytical exchange matrix elements are of the form:

$$\langle n,\sigma|H_{\rm exc}(K_Y)|n',\sigma'\rangle = C_O \int dQ_X \mathsf{F}[q_{X,Y}] f_n(Q_X)^* \times f_{n'}(Q_X) T_{\sigma,\sigma'}/q_{X,Y}, \quad (2)$$

where $C_O = (3/16)\Delta E_{LT}|\Psi_{1S}(0)/\phi_{3D}(0)|^2$; $\phi_{3D}(0)$ is the three-dimensional exciton envelope function at zero relative distance; ΔE_{LT} is the bulk longitudinal-transverse splitting; $q_{X,Y} = (Q_X^2 + K_Y^2)^{1/2}$; $T_{\sigma,\sigma'} = (Q_X - \sigma i K_Y)(Q_X + \sigma' i K_Y)$ and $f_n(Q_X)$ is the Fourier transform of $F_n(X)$. Equation (2) was obtained after averaging the bulk nonanalytical perturbation over the independent electron and hole confined motions in the well and over the $1S$-like relative motion for the electron/hole pair, like in the quantum well case, as well as over the $F_n(X)$ and $F_{n'}(X)$ CCM motions. Note that the exchange matrix element $\langle n,\sigma|H_{\rm exc}(K_Y)|n',\sigma'\rangle$ has both intra- ($n = n'$) and inter- ($n \neq n'$) confined level elements. Note also that for a given (n,n') pair, both spin-conserving ($\sigma = \sigma'$) and spin-mixing ($\sigma \neq \sigma'$) couplings are present. Note finally that the diagonal ($\sigma = \sigma'$) and spin-mixing ($\sigma \neq \sigma'$) terms do not necessarily vanish at $K_Y \to 0$. Altogether, these different contributions lead to the full energy dispersion $\varepsilon(K_Y)$ shown as solid lines in Fig. 1. (For clarity, in Fig. 1 the ground parabolic term $\varepsilon_1(K_Y)$ was subtracted from $\varepsilon(K_Y)$ and also only the first ten wire dispersions are shown.) In the following, we discuss separately these different contributions. In particular, the dashed curves in Fig. 1 represent the independent CCM dispersions discussed below.

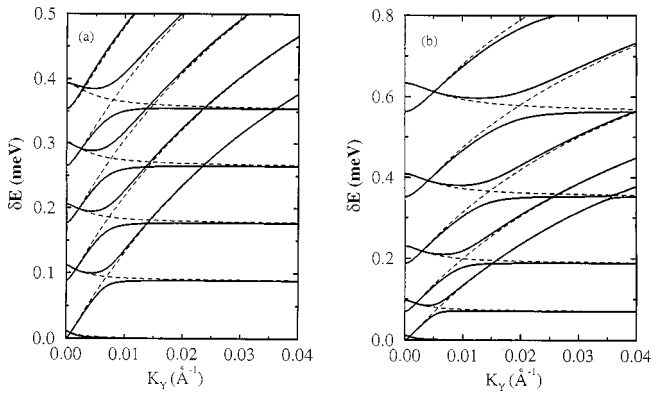

FIG. 1. Full lines: energy dispersions $\delta\varepsilon(K_Y) = \varepsilon(K_Y) - \varepsilon_1(K_Y)$ for a GaAs-based wire ($L_Z = 35$ Å). Dotted lines: independent CCM approximation. (a) Parabolic confinement: $L_X = 1000$ Å; $E_2 - E_1 = 0.088$ meV. (b) Square well confinement: $L_X = 3000$ Å; $E_2 - E_1 = 0.07$ meV.

Let us neglect initially the coupling between different CCM states ($n' = n$). In this approximation the wire states are spin mixed but have a well-defined X parity [the one of $F_n(X)$ for the nth independent subband]. The energies of the independent CCM dispersions are $\varepsilon_{n,\pm}(K_Y) = \varepsilon_n(K_Y) + \lambda_n(K_Y) \pm |\Lambda_n(K_Y)|$ with $\lambda_n(K_Y) = \langle n,\sigma|H_{\rm exc}(K_Y)|n,\sigma\rangle$ the diagonal and $\Lambda_n(K_Y) = \langle n,\sigma|H_{\rm exc}(K_Y)|n-\sigma\rangle$ the spin-mixing couplings. It is instructive to consider three particular situations.

(i) *Spin splitting at the subband edges.* First of all, note that at the subband edges ($K_Y \to 0$) the diagonal and spin-mixing couplings between the optically active ± 1 heavy excitons are equal and do not vanish: $\lambda_n(0) = \Lambda_n(0) \neq 0$. This is in striking contrast to the single quantum well case, where only moving excitons are spin mixed (linear-in-$K_\perp$ coupling). We find numerically that the resulting energy splitting $D_n = 2|\Lambda_n(0)|$ depends on n (it increases monotonously with n) and on the characteristic wire width L_X (it is roughly proportional to $1/L_X$). In fact, we have found numerically that $D_n \approx \sqrt{E_n}$ and that D_n is roughly equal to the exchange splitting of the single well states with $\mathbf{K}_\perp = (\pm Q_{X(n)}, K_Y = 0)$ where $Q_{X(n)}$ is such that $\hbar^2 {Q_{X(n)}}^2/2M = E_n$, namely, $Q_{X(n)} = {\eta_n}^{1/2}/L_X$. Thus, the splitting at the nth band edge is roughly equal to the one of the quantum well plane waves which most heavily contribute to the nth CCM stationary wire level.

(ii) *Intermediate K_Y states.* At $K_Y \neq 0$ the integrals involving the $\approx K_Y Q_X$ terms of $T_{\sigma,\sigma'}$ vanish and only the $Q_X^2 + K_Y^2$ (the $Q_X^2 - K_Y^2$) terms contribute to the diagonal (to the spin-mixing) part. Thus, the spin-conserving coupling energy increases monotonously with increasing K_Y. The spin-mixing term, on the contrary, initially decreases, vanishes at a given wave vector $K_Y = Q_{Y(n)}$, changes sign and increases again in absolute value when $K_Y \to \infty$. This result is in marked contrast with the single well situation, where the spin splitting increases monotonously with increasing $(Q_{X(n)}^2 + K_Y^2)^{1/2}$ for fixed $Q_{X(n)}$. Also, for finite wave vectors we obtain $|\lambda_n(K_Y)| \neq |\Lambda_n(K_Y)|$, in contrast again with the quantum well situation, where the diagonal and spin-mixing couplings are equal in absolute value for any $\mathbf{K}_\perp$ value. For $0 < K_Y \ll Q_{Y(n)}$ the spin splitting decreases roughly quadratically from its edge value: $2|\Lambda_n(K_Y)| \approx D_n - A_n(K_Y)^2$. At $K_Y = Q_{Y(n)}$ the spin coupling vanishes: $\Lambda_n(Q_{Y(n)}) = 0$, the two eigenenergies cross and the eigenvectors are, in this independent CCM model, pure ± 1 states, whereas they are completely mixed for $K_Y \neq Q_{Y(n)}$. We have found numerically that $Q_{Y(n)} \approx Q_{X(n)}$. The existence of the energy crossing at $Q_{Y(n)}$ can be traced back to the fact that in our structure the kinetic energy along the Y direction is comparable to the weak confinement energy due to the wire (while it is much smaller than the energy confinement along the quantum well growth axis).

(iii) *Large K_Y states.* Let us finally consider the behavior of the wire energies for large wave vectors: $K_Y \gg Q_{Y(n)}$. In this limit $|\lambda_n| \approx |\Lambda_n| \approx$ linear-in-K_Y and the spin splittings for the different decoupled CCM states are roughly the same and equal to the one linear-in-K_Y for the single underlying quantum well state with the same K_Y and $K_X \approx 0$. This is consistent with the fact that a perturbation in the real space with characteristic extent $\approx L_X$ principally affects the states in the reciprocal space within $\approx 1/L_X$.

It is interesting to point out that all these results for the independent CCM dispersions can be easily recovered within a simple frame, as follows. For the nth level, the $|f_n(Q_X)|^2$ terms in Eq. (2) are even in Q_X and heavily peaked around $Q_X \approx \pm Q_{X(n)}$. The exchange couplings are then roughly equal to

$$\langle n,\sigma|H_{\rm exc}(K_Y)|n,\sigma'\rangle \propto \mathsf{F}[q_{X(n),Y}]\{Q_{X(n)}^2 + \sigma\sigma' K_Y^2\}/q_{X(n),Y}, \tag{3}$$

with $q_{X(n),Y} = (Q_{X(n)}^2 + K_Y^2)^{1/2}$. This formula displays clearly the main characteristics of the energy dispersion discussed in the three situations above and, in addition, fits reasonably well the full numerical results shown as dashed lines in Fig. 1 (the agreement is better for the vertical confinement case).

It is worth noticing that the exchange coupling at finite K_Y can become larger than the center-of-mass confinement energy due to the wire. This leads to a series of energy crossings between levels belonging to different CCM subbands: for instance, the high energy spin-mixed level of the nth subband and the low energy one of the mth subband, with $m > n$: $\varepsilon_{n,+}(K_Y) = \varepsilon_{m,-}(K_Y)$. Let us consider now the exchange-induced couplings between different CCM states ($n' \neq n$). We distinguish two contributions: the term diagonal in spin $T_{\sigma,\sigma}$ and the term in $Q_X^2 - K_Y^2$ of $T_{\sigma,-\sigma}$ couple states of the same X parity, whereas the terms in $K_Y Q_X$ of $T_{\sigma,-\sigma}$ couple states of different parities. We can nevertheless show on general grounds that only the latter can lift the energy degeneracy at $K_Y \neq 0$ between two levels of different independent CCM states. This means that only the crossings between levels of CCM subbands with different parities are possibly lifted. More than that, since they are roughly proportional to the intersubband ''velocity'' matrix element $V_{n,m} = \langle F_n(X)|-\partial/\partial X|F_m(X)\rangle$, we find that in the case of a parabolic wire, only the energy crossings between consecutive oscillators (those between any two states with different parities for a vertical wire) are replaced by anticrossings. These trends are observed in Fig. 1. In conclusion, in spite of the fact that the full dispersions in Fig. 1 are complicated, their main qualitative aspects can be satisfactorily anticipated by just considering a few intra- and intersubband exchange-related couplings. Note finally that in the absence of the $V_{n,m}$ terms, the CCM wire states would have a well-defined parity. Both the quantum well plane-wave limit for the envelopes along the x direction and the linear-in-$K_\perp$ quantum well spin splitting can only be properly recovered at $L_X \to \infty$ when these spin- and parity-mixing couplings are accounted for.

III. WEAKLY CONFINING WIRES: SPIN DEPOLARIZATION

The $\sigma = \pm 1$ pure spin levels are not eigenstates of the full Hamiltonian with exchange interaction. An exciton initially in the $|n_i;\sigma_i;K_Y\rangle$ state would evolve in time because of the intra- and the intersubband couplings. The former leads to a harmonic evolution with frequency $|\Omega_n(K_Y)|$, where $\Omega_n(K_Y) = 2\Lambda_n(K_Y)/\hbar$. The latter render the time evolution more complex. Let us here neglect the intersubband terms (a fair approximation for not too wide wires) and consider the

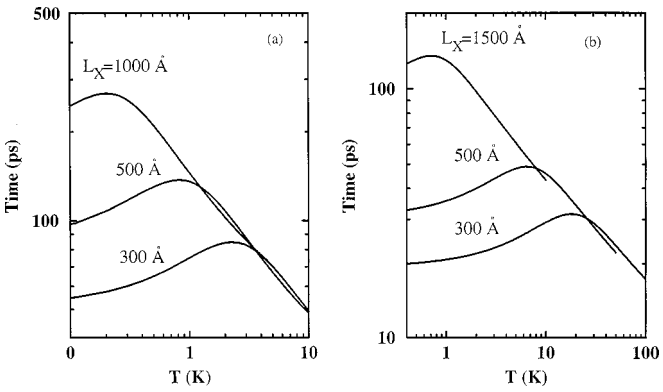

FIG. 2. Temperature dependence of the average spin-flip time for a thermal distribution of excitons in the independent CCM approximation (see text) for different parabolic (a) or vertical (b) wires. $L_Z = 35$ Å.

average spin-flip rate for nondegenerate gas of independent free excitons:

$$\langle|\Omega_{\text{intra}}|\rangle = \sum_i |\Omega_i| \exp\{-\beta\varepsilon_i\} \Big/ \sum_i \exp\{-\beta\varepsilon_i\}, \quad (4)$$

where the summations are performed over all the subbands and wave vectors: $i=\{n,K_Y\}$, $\varepsilon_i=\varepsilon_n(K_Y)$, and $\Omega_i = \Omega_n(K_Y)$. We show in Fig. 2 the temperature dependence of the spin-flip time defined as $\pi/\langle|\Omega_{\text{intra}}|\rangle$ for different wires. Note that all the curves display the same qualitative variation, namely, the average time initially increases slowly, reaches a maximum value and thus decreases with increasing temperature. The presence of the maximum is due to the vanishing of the spin coupling at a given finite K_Y value. The temperature for the maximum time is roughly proportional to the CCM confinement energy and is larger for the vertical confinement case [Fig. 2(b)]. These trends can be fully understood if we consider the average depolarization rate for the ground independent subband within the approximation given in Eq. (3). In this case, $n=1$ in Eq. (4) and the average spin-flip time defined as $\tau = \pi/\langle|\Omega_{\text{intra}(n=1)}|\rangle$ reads

$$\tau(0)/\tau(T) = 2[a/\pi]^{1/2} \int dx F[Q_{X(1)}(1+x^2)^{1/2}] \times \exp\{-ax^2\}|1-x^2|/[1+x^2]^{1/2}, \quad (5)$$

with $a=E_1/K_BT$ and $\tau(0)=\pi/|\Omega_1(0)|$. We present as a solid line in Fig. 3 the temperature dependence of the ratio $\tau(T)/\tau(0)$. We take $F[q]=1$ in this figure. In this case, at low temperature ($a \gg 1$) we have approximately $\tau(T)/\tau(0) \approx 1+3/(4a)$ and at high temperature ($a \ll 1$), there is $\tau(T)/\tau(0) \approx [\pi a]^{1/2}$. These results are shown, respectively, as dotted and dashed lines in Fig. 3. Thus, the spin-flip time $\tau(0)=\hbar/D_1 \propto L_X$ is finite at $T=0$ K, increases slightly with T at low temperatures, reaches a maximum near $T_M = E_1/K_B \propto 1/L_X^2$, and then decreases like $T^{-0.5}$ at high temperatures. These approximate results fit quite well the full calculated curves in Fig. 2. Note, however, that the solid line in Fig. 3 approaches its asymptotic decrease at high temperature rather slowly. In fact, for $1 \ll K_BT/E_1 \leqslant 100$, its decrease is best fitted by a $T^{-0.6}$ law.

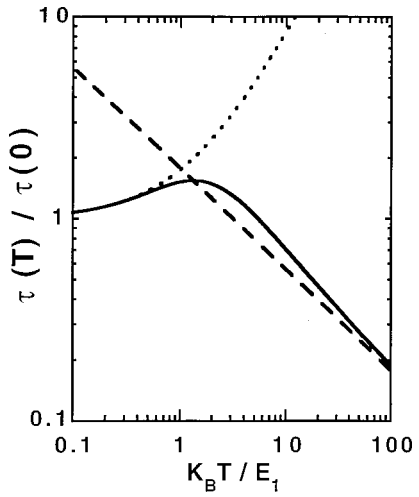

FIG. 3. Average spin-flip time for a thermal distribution of excitons in the ground independent CCM subbands (see text).

It is well known that scattering processes sensitively affect the spin-depolarization rate of free carriers and excitons in bulk[11] and quantum wells.[2,3,12] Let us consider their importance on the spin relaxation of excitons in quantum wires. The full problem is quite complex, because the disorder and the exchange perturbations have both intrasubband and intersubband couplings. In the following we discuss three limiting situations for the time evolution of the polarization in the presence of spin-conserving elastic scatterings and spin-flip exchange couplings: (i) exchange and scattering in the independent CCM model; (ii) intersubband scattering among the different subbands and intrasubband exchange coupling; (iii) intersubband exchange coupling and intrasubband scattering processes.

(i) Independent CCM subbands. Let us initially focus on the one-subband model. An elastic scattering can only change the sign of K_Y. Since for $n=n'$ the spin-mixing coupling depends only upon $|K_Y|$, no interference is possible between the spin precession and the center-of-mass motion in the presence of scatterers, which in bulk and quantum wells leads to the well known D'yakonov-Perel mechanism for the spin relaxation.[11] This means that the total spin polarization at $\pm|K_Y|$ never decays but oscillates in time with a period proportional to $1/|\Omega_n(K_Y)|$. In a semiclassical picture, the exciton spin precesses around an effective magnetic field $\Omega_n(|K_Y|)\hat{\mathbf{e}}_\mathbf{x}$ pointing always along the x direction, independently of its propagation direction along the wire axis. In other words, in the independent CCM picture the spin-depolarization rate is not affected by the elastic scatterings. This result is in sharp contrast with the single quantum well case where such scatterings sensitively modify the spin depolarization rate as compared to the situation without disorder.[2,3,12] It can be understood if we remember that even in quantum wells the depolarization rate remains unaffected by the forward and backward ($K_\perp \leftrightarrow -K_\perp$) scattering processes, which leaves unchanged the spin-mixing effective magnetic field: the irreversible (D'yakonov–Perel-like) depolarization appears because of the scatterings in different in-plane directions, which processes become quenched in quantum wires because of the confinement along the x direc-

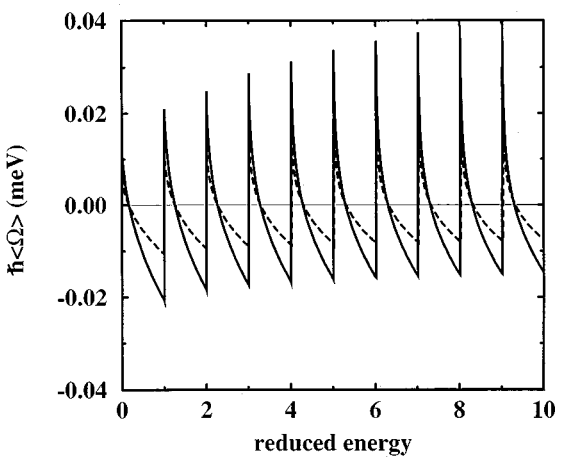

FIG. 4. Energy dependence of the average effective field $\langle\Omega\rangle$. Parabolic wire: $L_X=500$ Å (full line) and 1000 Å (dashed lines). $L_Z=35$ Å. The reduced energy is $[\varepsilon-E_1]/(E_2-E_1)$.

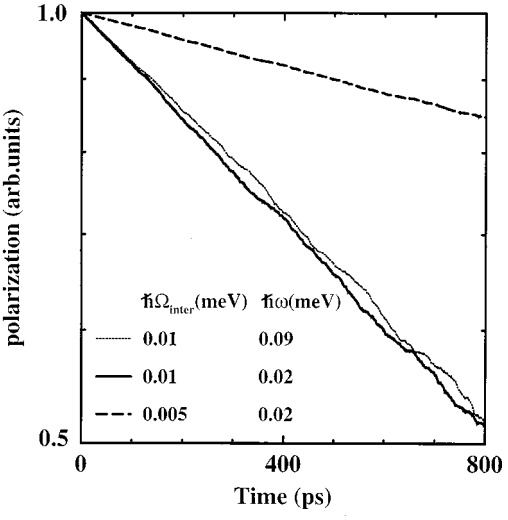

FIG. 5. Numerical simulation of the time evolution of the spin polarization (vertical log scale) within the four-level model (see text) in the presence of assisted scattering ($\tau^*=2$ ps) and for different Ω_{inter} and ω values.

tion. Finally, for a gas of independent excitons, the average spin-flip rate in the presence of disorder is equal to the one for free excitons [Eq. (4)].

(ii) Role of the intersubband scatterings. Let us discuss now how the disorder induced coupling between different CCM motions affects the spin depolarization. Because of the elastic processes $|n,K_{Y(n)},\sigma\rangle\rightarrow|n'\neq n,K'_{Y(n')},\sigma'=\sigma\rangle$, an exciton spends its time among the different levels at constant energy. The random sequence of intersubband scattering events gives rise to a random variation of the exciton wave vector and thus of the magnitude and direction of the effective magnetic field $\Omega_n(|K_Y|)\hat{\mathbf{e}}_\mathbf{x}$ ''seen'' at each subband. In fact, as shown above, for fixed n, the sign of the spin-coupling term $\Lambda_n(K_Y)$ changes at K_n, so that for a fixed exciton total energy the effective fields can have different signs for different subbands. As a consequence, in the regime of frequent elastic intersubband scatterings, the mean spin-mixing coupling ''felt'' by one exciton with fixed total energy ε is $\langle\Omega(\varepsilon)\rangle=\Sigma_n\Omega_n(K_{Y(n)})P_n/\Sigma_nP_n$, where $P_n=\theta[\varepsilon-\varepsilon_n(0)]/K_{Y(n)}$ is proportional to the one-dimensional density of states of the nth parabolic subband at the exciton energy $\varepsilon_n(K_{Y(n)})=\varepsilon$ and θ is the step function. We show as solid lines in Fig. 4 $\langle\Omega(\varepsilon)\rangle$ as a function of the reduced energy $[\varepsilon-E_1]/(E_2-E_1)$ for two parabolic wires: $L_X=500$ and 1000 Å. In the semiclassical picture, $\langle\Omega(\varepsilon)\rangle\hat{\mathbf{e}}_\mathbf{x}$ plays the role of a mean effective field around which the exciton spin precesses. The spin evolution takes place in the z-y plane, since $\Omega_n(K_Y)\hat{\mathbf{e}}_\mathbf{x}$ always points out along the (positive or negative) x axis. As a consequence, the polarization lost in one subband would be partly recovered after one scattering which reverses the sign of the effective field. We can show that at time $\tau_N=N\tau^*$ (after N collisions) the semiclassical z component of the spin, $S(\tau_N)$, reads in the frequent scattering regime:

$$S_Z(\tau_N)=S_Z(0)\exp\{-\tau_N/\tau_S\}\cos[\langle\Omega(\varepsilon)\rangle\tau_N], \qquad (6a)$$

$$2/\tau_S(\varepsilon)\approx\langle[\Omega(\varepsilon)-\langle\Omega(\varepsilon)\rangle]^2\rangle\tau^*. \qquad (6b)$$

Thus, in the general case, the time evolution is harmonically damped. For the exciton energies where the mean field vanishes, the spin polarization decays with the rate $\langle\Omega^2\rangle\tau^*/2$. Such inhibition of the spin depolarization in the frequent scattering regime is due to the interplay between scattering and spin coupling for an ensemble of independent wire subbands. This interplay is at the origin of the motional narrowing effect which characterizes the D'yakonov–Perel-like irreversible spin relaxation in single wells.[11] In fact, both the amplitude and the energy period of the oscillations in Fig. 4 decrease when the wire confinement decreases: for a fixed reduced exciton energy $[\varepsilon-E_1]/(E_2-E_1)$, one finds that $\langle\Omega\rangle\rightarrow0$ when $L_X\rightarrow\infty$. In addition, for a fixed exciton energy ε, we can show that the mean field goes to zero, in agreement with the isolated well situation, where the in-plane angular average vanishes for a fixed in-plane kinetic energy. The mean squared coupling $\langle\Omega^2(\varepsilon)\rangle$, on the contrary, remains finite when $L_X\rightarrow\infty$ [these two results can be readily obtained by using Eq. (3) with $\mathsf{F}[q_{X(n),Y}]\approx1$]. In conclusion, Fig. 4 and Eq. (6) show that the spin-flip process due to the disorder-induced coupling between different CCM motions is enhanced with increasing wire confinement, since both $|\langle\Omega(\varepsilon)\rangle|$ and $\langle\Omega^2(\varepsilon)\rangle$ increase when L_X decreases.[13]

(iii) Role of the intersubband exchange couplings. Finally, a motional narrowinglike relaxation of the exciton polarization is obtained when we consider the intersubband exchange coupling between states with the same K_Y in the presence of intrasubband assisted scatterings. In fact, as shown above, a linear-in-K_Y coupling exists between CCM states with different parities and spins. This implies, in particular, the existence of a nonvanishing interference between, say, the states $|A\rangle=|n,\sigma,K_Y\rangle$ and $|B\rangle=|n+1,-\sigma,-K_Y\rangle$, corresponding to the two different paths connecting $|A\rangle$ to $|B\rangle$: (i) one elastic scattering followed by the intersubband coupling at $-K_Y$ and (ii) one intersubband coupling at $+K_Y$ followed by one scattering inside the $n+1$ dispersion. We show in Fig. 5 the results for the time-evolution of the polarization obtained by solving numerically the coupled set of equations

for the 4×4 density matrix for two coupled CCM motions (four level model: $|n,\pm1\rangle$ and $|n+1,\pm1\rangle$). The scattering is accounted for by introducing a random variation of the sign of K_Y with probability $1/\tau^*$, when solving the free evolution inside each consecutive interval $\Delta t \ll \tau^*$ (assuming for simplicity the same scattering probability for the two subbands). We see clearly that the polarization decreases exponentially to zero in the strong scattering regime ($\Omega_{\text{inter}}\tau^* \ll 1$), where the spin relaxation time τ_S is roughly given by

$$1/\tau_S = (1/2)\,\tau^*(\Omega_{\text{inter}})^2/[1+(\tau^*\omega)^2], \tag{7}$$

with $\hbar\Omega_{\text{inter}}$ the inter-CCM linear-in-K_Y coupling energy. We recognize the inhibition of the depolarization due to the energy separation $\hbar\omega$ of the interacting ''up'' and ''down'' levels. These results emphasize the existence of two couplings governing the spin depolarization in this regime, namely, the spin-mixing intersubband coupling and the spin-conserving intrasubband scatterings. We can show that Eq. (7) leads to a constant rate $1/\tau_S$ when $L_X\to\infty$ and $n\to\infty$ for fixed K_Y and fixed exciton energy (i.e., with η_n/L_X^2 constant), as expected for the isolated well limit. We have also obtained that for fixed n and K_Y the spin-flip rate increases when L_X decreases in the weak confinement regime, in spite of the fact that $\hbar\omega$ also increases.[14]

Let us finally stress a last point concerning the wire states. We have assumed up to this point that the wire confinement was along the X axis. Let us consider now a confinement along an arbitrary axis in the (χ,Y) plane and define the (X',Y') frame with X' along the new confinement direction and Y' the new wire axis. In this new frame the exchange coupling interaction is exactly the same as in Eq. (2) (with $Y\to Y'$ and $X\to X'$) except for a multiplicative constant phase factor equal to $\exp\{i(\sigma-\sigma')\alpha\}$, where α is the angle between the X and X' axis. Consequently, the energy dispersions (and the absolute value of the spin couplings) do not depend upon α. Concerning the spin-depolarization effects discussed above, the new effective field around which the spin precesses always has the same magnitude but points out along a different direction. When the confinement axis is Y, $\alpha=\pi/2$, the spin-splitting changes sign and the effective field points out along the opposite direction with respect to the one obtained for a confinement along X. For $\alpha=\pi/4$, it points out along the Y direction and so on... . The depolarization mechanisms discussed above are however insensitive to the value of α.

In conclusion, we summarize our results for the exciton spin states in weakly confining wires. (i) In the absence of scatterings, K_Y is a good quantum number and the stationary states are mixed spin levels forming complicated dispersion subbands. (ii) When the intersubband couplings are neglected, we find in the time domain that the spin oscillates irrespective of possible intrasubband elastic scatterings. (iii) When elastic intersubband scatterings are considered and the intersubband exchange couplings are neglected, the semiclassical time evolution for the exciton spin is harmonically damped: it oscillates around an effective average field which points along the wire confining axis and whose direction and magnitude depend upon the exciton energy. The depolarization rate is inversely proportional to the scattering one. (iv) A motional narrowinglike contribution to the relaxation of the spin polarization appears also when the intersubband exchange couplings are considered in the presence of intrasubband assisted scatterings. For the study of the spin-depolarization of a distribution of photoexcited excitons, a more detailed model, incorporating simultaneously these different contributions, is necessary; this is, however, beyond the scope of this paper. Our main aim here was to discuss the three contributions to the spin depolarization, which all increase when the (weak) wire confinement increases.

IV. STRONG CONFINING WIRES

We are interested here in the low-lying exciton states associated to the first interband transition. The corresponding electron and hole levels are confined by the wire potentials along the z and x directions (the wire axis is taken as before along the y direction). In order to evaluate the role of these strong (vertical) confinements on the spin properties we assume in the following that the conduction and valence discontinuities in both z and x directions are infinite. The motions along z and x are then separable and, in the absence of exchange interaction, the low-lying heavy exciton (pure spin) levels of the wire read

$$\Psi = \phi(z_e)\chi(z_h)\xi(x_e)\,\eta(x_h)\Phi_{1S}(y)\exp(iK_YY)/\sqrt{L_Y}, \tag{8a}$$

$$\varepsilon_n(K_Y) = E_e+E_h+E_x-E_{1S}+\hbar^2K_Y^2/2M, \tag{8b}$$

where the first two and the last terms are the same as in Eq. (1). The third and fourth terms account for the wire confinements (total energy confinements $E_x=\hbar^2\pi^2/(2\mu L_X^2)$ for the electron-hole pair). We assume for the relative motion the variational wave function: $\Phi_{1S}(y)=N_\lambda\exp(-y^2/\lambda^2)$ where λ is the variational parameter and N_λ the normalization constant.[15] The heavy states in Eq. (8) are fourfold degenerate when we consider the electron and hole spins ($\sigma=\pm1$, ±2 for the z component of the exciton spin). For a given wire (fixed ϕ, χ, ξ, η, and Φ_{1S}) the quantum wire states are specified by two quantum numbers, $|\sigma;K_Y\rangle$, and form a parabolic dispersion as a function of K_Y.

Following the same lines leading to Eq. (2), the nonanalytical exchange matrix elements in the strong confinement regime are of the form

$$\langle\sigma|H_{\text{exc}}(K_Y)|\sigma'\rangle = C_1\int dQ_X \mathsf{F}[q_{X,Y}]|f(Q_X)|^2 \times\{Q_X^2+\sigma\sigma'K_Y^2\}/q_{X,Y}, \tag{9a}$$

$$f(Q_X) = \langle\xi(x)|\exp\{iQ_Xx\}|\eta(x)\rangle = \sin(\theta_X)/[\theta_X(1-\theta_X^2/\pi^2)], \tag{9b}$$

where $C_1=(3/32\pi)\Delta E_{LT}|\Phi_{1S}(0)/\phi_{3D}(0)|^2$, $\theta_X=Q_XL_X/2$ and the other quantities are defined in Sec. II. The diagonal and the spin-mixing couplings in Eq. (9) differ from the corresponding ones in Eq. (2) by the multiplicative constant related to the relative motion and by the function $f(Q_X)$ in

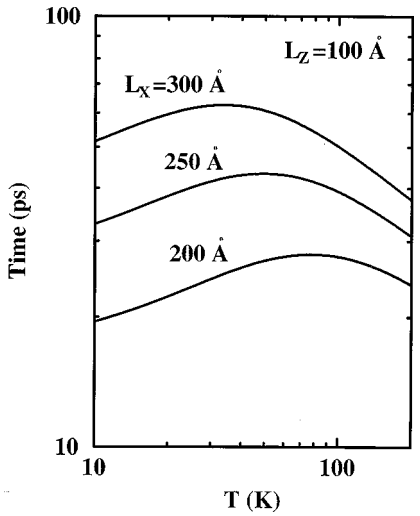

FIG. 6. Temperature dependence of the average spin-flip time for a nondegenerate exciton gas in different vertical wires: $L_Z = 100$ Å and $L_X = 200$ Å (lower), 250 Å (middle), and 300 Å (upper curve).

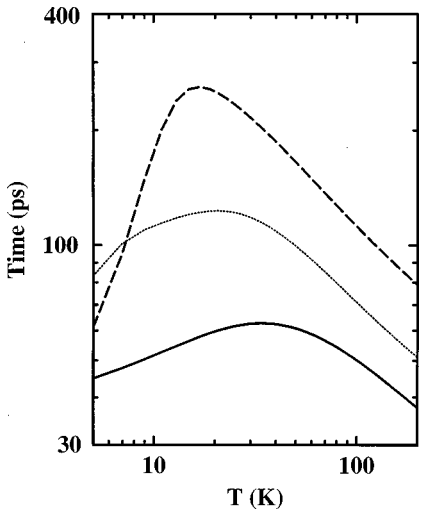

FIG. 7. Temperature dependence of the spin-flip time for different broadenings and potential depths. Solid line: $\gamma = 0$. Dotted line: $\gamma = 1.5$ meV; $V_0 = 5$ meV. Dashed line: $\gamma = 3$ meV; $V_0 = 10$ meV. $L_X = 300$ Å and $L_Z = 100$ Å.

the integral. However, most of the qualitative discussion presented in Sec. II within the independent CCM subbands model apply also for the present CEH case. In particular, it follows from Eq. (9) that the exchange splitting is finite at the subband edge, decreases and vanishes at a particular K_Y value and then increases again in absolute value with increasing K_Y. We obtain also similar results for the spin depolarization rate, as shown in Fig. 6 where we show the temperature dependence of the mean spin-flip time for different wire parameters ($L_Z = 100$ Å and $L_X = 200$, 250, and 300 Å) calculated using Eq. (4) with $n = 1$. We note the same qualitative behavior as in Figs. 2 and 3. For fixed L_Z, the spin splitting at both $K_Y = 0$ and large K_Y values are inversely proportional to L_X. This explains why the low temperature and the high temperature asymptotes in Fig. 6 are L_X dependent.

Nishimura *et al.*[16] and Sogawa *et al.*[17] have performed experimental studies of the spin-depolarization rate in quantum wires. The first authors measured a smaller exciton depolarization time in the wires with respect to a single well and obtained qualitatively the same variation as a function of the temperature for the spin-flip time as the ones in Figs. 2, 3, and 6. Their times for a strongly confining wire are, however, larger (maximum value for the spin-flip time $\approx$500–600 ps) than the ones we have calculated. The second authors measured a spin-flip time which decreases quasimonotonously in the investigated temperature range. In addition, the measured relaxation time is longer in quantum wires with respect to the one in a single quantum well. These discrepancies can be due to the presence of disorder in the structures investigated.[18] First, the wire-to-well comparison between the spin-flip times are haphazard, since the quantum well depolarization is in the general case sample dependent.[2,3,12] Second, the results of the two groups for the wire structure can equally be affected by the sample quality. The proper analysis of the role played by the defects on the spin depolarization is beyond the scope of this work.[19] We consider here, nevertheless, very briefly the role of localization in the spin depolarization of the wire excitons within a crude model. We assume the presence of weak attractive defects which are able to bind the exciton center-of-mass along the wire axis. In this case, we can evaluate to the lowest order the spin-mixing perturbation which lifts the spin degeneracy of the bound states:

$$\Delta E(\ell_Y) = \Sigma_{K_Y} |g(K_Y;\ell_Y)|^2 \Delta E(K_Y), \tag{10}$$

where $\Delta E(K_Y)$ is the spin splitting for free wire excitons [see, e.g., Eq. (9)], $g(K_Y;\ell_Y)$ is the Fourier transform of the bound level envelope, and ℓ_Y its characteristic spatial extension. The important point which clearly follows from Eq. (10) is that the spin splittings of the quasizero-dimensional bound exciton states do not vanish in the general case since $\Delta E(K_Y)$ is an even function of K_Y, but can be positive or negative depending on the localization length ℓ_Y (for fixed L_X and L_Z thicknesses[20]). In order to illustrate this point, we assume a Gaussian-like form for the bound level envelopes. In addition, we take the rough dependence $\varepsilon_Y \approx -V_0 + \hbar^2/2M\ell_Y^2 < 0$ for the binding energy in a potential of depth V_0. This follows the work by Bellessa *et al.*,[18] where the localization effects are mainly associated to the presence of defects with same depth (the one due to a one-monolayer fluctuation) but with different widths along the wire axis. We have found numerically that the spin-splitting is positive for the deeper states localized in large defects (large ℓ_Y), decreases when ℓ_Y decreases and can become negative for the states localized in narrower defects, depending on the potential depth V_0. This can be qualitatively understood as follows: the deeper levels (localized in wider defects) are mainly formed from small K_Y plane waves, which have a positive splitting, whereas shallow levels (localized in narrow defects) contain also contributions of free states with negative splitting. In the evaluation of the average spin-depolarization rate for a thermal distribution of excitons, we should also consider in Eq. (4) the contribution of the bound levels. For that we use a model one-dimensional density-of-states: $\rho(\varepsilon_Y) = \exp\{-(\varepsilon_Y/\gamma)^2\}/\sqrt{\gamma}$ for $\varepsilon_Y \leq 0$ and $\rho(\varepsilon_Y)$

$=1/\{\varepsilon_Y^2+\gamma^2\}^{1/4}$ for $\varepsilon_Y \geqslant 0$, where γ is the broadening parameter. We present in Fig. 7 the temperature dependence of the spin-flip time for different broadenings and potential depths ($L_X=300$ Å; $L_Z=100$ Å). For comparison, we redraw the $\gamma=0$ curve (solid line) from Fig. 6. We observe that the presence of defects leads to a rather different temperature dependence for the average spin-flip rate. In particular, it *increases* the mean depolarization time.

In conclusion, we believe that the mechanisms we have discussed in this work are pertinent for the understanding of the dynamics of the spin depolarization for *free* excitons in quantum wires. In addition, we have shown in the frame of a simple model that the localization effects can sensitively affect the spin depolarization for excitons in *actual* quantum wires.

ACKNOWLEDGMENTS

It is a pleasure to thank G. Bastard, J. Bellessa, R. Grousson, Ph. Roussignol, and V. Voliotis for fruitful discussions. D.L. was supported by DGA/DSP (France). The Laboratoire de Physique de la Matière Condensée is ''Unité de Recherche Associée au CNRS (URA 1437) et aux Universités Paris 6 et 7.''

[1] L. C. Andreani, in *Confined Electrons and Photons, New Physics and Application*, Vol. 340 of *Nato Advanced Study Institute, Series B: Physics*, edited by E. Burstein and C. Weisbuch (Plenum, New York, 1995).

[2] M. Z. Maialle, E. A. De Andrada e Silva, and L. J. Sham, Phys. Rev. B **47**, 15 776 (1993).

[3] A. Vinattieri, J. Shah, T. C. Damen, D. S. Kim, L. P. Pfeiffer, M. Z. Maialle, and L. J. Sham, Phys. Rev. B **50**, 10 868 (1994); L. Muñoz, E. Pérez, L. Viña, and K. Ploog, *ibid.* **51**, 4247 (1995); T. Amand, D. Robart, X. Marie, M. Brousseau, P. Le Jeune, and J. Barrau, *ibid.* **55**, 9880 (1997).

[4] Strictly speaking, only the $K_Y=0$ states are optically active. We retain, however, the term ''active'' for all heavy levels within the $\sigma=\pm 1$ dispersions.

[5] In the following, we call ''linear-in-$K_\perp$'' the single well exchange coupling, even though it is roughly linear only for $K_\perp \ll 1/L_Z$ with L_Z the well width. For $K_\perp \geqslant 1/L_Z$, the form factor $\mathsf{F}(K_\perp)$ weakens the increasing of the splitting with $K_\perp$.

[6] See, for instance, P. Ils, M. Michel, A. Forchel, I. Gyuro, M. Klenk, and E. Zielinski, Appl. Phys. Lett. **64**, 496 (1994).

[7] A. Gustafsson, F. Reinhardt, G. Biasiol, and E. Kapon, Appl. Phys. Lett. **67**, 3673 (1995).

[8] S. Jaziri, R. Ferreira, R. Bennaceur, and G. Bastard, Nuovo Cimento D **17**, 1513 (1995).

[9] G. Bastard, *Wave Mechanics Applied to Semiconductor Heterostructures* (Editión de Physique, Les Ulis, 1988).

[10] G. E. Pikus and G. L. Bir, Zh. Eksp. Teor. Fiz. **60**, 195 (1971) [Sov. Phys. JETP **33**, 108 (1971)].

[11] See, for instance, M. I. D'yakonov and V. I. Perel, in *Modern Problems in Condensed Matter Sciences*, Vol. 8 of *Optical Orientation*, edited by F. Meier and B. Zakharchenya (North-Holland, Amsterdam, 1984).

[12] See, for instance, M. I. D'yakonov, and V. Yu. Kachorovskii, Fiz. Tekh. Poluprovodn. **20**, 178 (1986) [Sov. Phys. Semicond. **20**, 110 (1986)]; G. Bastard and R. Ferreira, Surf. Sci. **267**, 335 (1992).

[13] We neglect the dependence of the scattering matrix elements with the wave-vector variation ΔK_Y. The intersubband scattering involves larger wave-vector variations when L_X decreases.

[14] Note, however, that the scattering time τ^* is possibly a function of L_X.

[15] This variational wave function is, of course, unable to describe the extreme one-dimensional situation where $L_{X,Z} \to 0$, but, hopefully, it is accurate enough for realistic wire thicknesses.

[16] T. Nishimura, X. L. Wang, M. Ogura, A. Tackeuchi, and O. Wada, in *Workbook of the Third Symposium on the Physics and Application of Spin-Related Phenomena in Semiconductors* (Sendai, Japan, 1997).

[17] T. Sogawa, S. Ando, H. Ando, and H. Kanbe, in *Workbook of the Third Symposium on the Physics and Application of Spin-Related Phenomena in Semiconductors* (Ref. 16).

[18] J. Bellessa, V. Voliotis, R. Grousson, X. L. Wang, M. Ogura, and H. Matsuhata, Phys. Rev. B **58**, 9933 (1998).

[19] D. Larousserie and R. Ferreira (unpublished).

[20] After completion of our work, we became aware of one paper by Gupalov *et al.* {S. V. Gupalov, E. L. Ivchenko, and A. V. Kavokin, Zh. Eksp. Teor. Fiz. **86**, 703 (1998) [JETP **86**, 388 (1998)]} concerning the theoretical study of the fine structure of quantum well states corresponding to excitons localized in large interface defects. We obtain qualitatively the same results for the exchange splitting of localized excitons if we use in Eq. (10) the couplings given in Eq. (2) or Eq. (3) for the case of a center-of-mass confinement along the *X* and *Y* directions. In particular, we obtain also a splitting which for a fixed L_Z value is negative when $L_Y/L_X<1$, vanishes for $L_Y=L_X$ and becomes positive for $L_Y/L_X>1$.